Meas. Sci. Technol. **18** (2007) 2067–2073 doi:10.1088/0957-0233/18/7/037

Correction factors for 4-probe electrical measurements with finite size electrodes and material anisotropy: a finite element study

E J Zimney[1], G H B Dommett, R S Ruoff and D A Dikin

Department of Mechanical Engineering, Northwestern University, Evanston, IL 60208, USA

E-mail: r-ruoff@northwestern.edu and d-dikin@northwestern.edu

Received 7 March 2007, in final form 11 April 2007
Published 12 June 2007
Online at stacks.iop.org/MST/18/2067

Abstract
In four-probe (4-probe) electrical measurements, especially on highly resistive materials, it is not always possible to configure the electrodes such that the current density is uniform throughout the sample. Under such circumstances, simply considering the material's electrical resistivity to be proportional to the measured resistance with the proportionality constant given by the sample geometry can give an incorrect result. In this paper, a numerical finite element model is presented which can extract a material's *true* resistivity from co-linear 4-probe electrical measurements on highly resistive samples with large electrodes that extend across the sample width. The finite element model is used to investigate the influence of material anisotropy, the resistance of the sample–electrode interfaces and the relative electrode-to-sample size on the potential and current density distributions in the sample. A correction factor is introduced to account for the impact of these effects on the measured resistivity. In the limit of large interface resistance, excellent agreement is found with an analytical expression derived elsewhere (Esposito *et al* 2000 *J. Appl. Phys.* **88** 2724–9). The approach presented here can be used to evaluate a variety of effects on co-linear 4-probe electrical measurements, can be extended to complex specimen geometries with arbitrary electrode arrangements and, additionally, could find use in the evaluation of data from 4-probe thermal conductivity measurements.

Keywords: electrical resistance, four-probe method, anisotropy, interface resistance, correction factor, finite element model

(Some figures in this article are in colour only in the electronic version)

1. Introduction

The direct current electrical resistance measurement is a routine method of characterizing the electrical properties of bulk materials, and many experimental methods have been developed [1]. A common experimental technique is the co-linear four-probe (4-probe) method. This configuration (see figure 1) consists of four independent electrical terminals where two terminals are used to apply current to the sample, and the other two terminals measure the resulting potential drop across a defined portion of the specimen. Provided a high impedance voltmeter is used to measure the potential drop, the 4-probe arrangement *under ideal conditions* (i.e. point electrodes) prevents current from flowing through the

[1] Now at Boeing Commercial Airplanes, Seattle, WA, Eric.J.Zimney@Boeing.com.

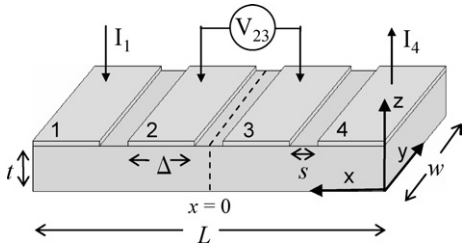

Figure 1. Schematic of the co-linear 4-probe configuration with electrodes that span the width of the specimen.

interface between the sample and the potential leads, thus eliminating interface resistance from the measurement.

A material's resistivity can be calculated from the measured 4-probe resistance $\left(R_{ij}^{kl}\right)$, the sample dimensions and the relative positions of the electrodes (assuming electrodes with zero width) by the following relationship:

$$\rho_{\mathrm{m}} = \frac{wt}{s} R_{ij}^{kl} = \frac{wt}{s} \frac{V_{kl}}{I_{ij}}\,, \tag{1}$$

where w, s and t are the sample width, inter-electrode spacing and sample thickness respectively, I_{ij} is the current applied to the i and j electrodes and V_{kl} is the measured potential drop across the k and l electrodes. In equation (1), it is assumed that there is a linear potential field distribution (i.e. uniform current density distribution) within the sample. In this work, the resistivity computed using equation (1) is referred to as the *measured* resistivity, ρ_{m}.

Performing electrical measurements on highly resistive materials is difficult due to the challenge of getting sufficient current into the specimen to ensure that the resulting potential drop is measurable. This often requires the use of large electrodes that are close together. In such cases, current can flow through the highly conductive electrodes and perturb the current and potential field distributions within the sample. Perturbations to the potential and current density fields can also be the result of the geometry of the specimen, material anisotropy, value of the electrode–sample interface resistance, inhomogeneous properties and any other nonlinear effects that may occur. A correction factor $\left(F_{ij}^{kl}\right)$ is often added to equation (1) $\left(\rho = F_{ij}^{kl}\rho_{\mathrm{m}}\right)$ to account for the effect of these perturbations in the calculation of the material's true resistivity (ρ). Correction factors for the 4-probe method with point electrodes on isotropic materials have been investigated extensively [2–7].

In this paper we report a method based on numerical finite element (FE) analysis, to determine correction factors for the analysis of co-linear 4-probe electrical measurements on isotropic and anisotropic samples with large, highly conductive electrodes that extend across the sample width. The results of the FE analysis in the limiting case of large interface resistance are compared with an analytical expression derived elsewhere [8–10]. All FE analysis was carried out using the Comsol Multiphysics 3.2 software package (Comsol, AB).

2. Analysis method

The FE analysis presented here is based on the formulation of a linear conductivity model that obeys local electrodynamics and assumes that the material being interrogated has a linear *I–V* relationship and is homogeneous. The electrical potential field distribution, $V(x, z)$, is governed by Laplace's equation, $-\vec{\nabla} \cdot [(\rho^{-1})\vec{\nabla} V] = 0$. Since the electrodes span the entire width of the specimen, the potential and current density fields are constant along the sample width (y-axis, see figure 1), and a two-dimensional (2D) model is sufficient.

2.1. Material anisotropy

Here we consider anisotropic materials where the in-plane resistivity ($\rho_x = 1$) differs from the transverse resistivity (ρ_z). Such anisotropy is common in many materials such as graphite [11], layered chalcogenides [12], perovskites [8, 10, 13], artificial super lattices, some biological tissues [14, 15], polymer composites [16, 17], among others. For an anisotropic material, the 2D Laplace's equation can be rewritten as

$$\xi(\partial^2 V/\partial x^2) + (\partial^2 V/\partial z^2) = 0, \tag{2}$$

where $\xi = \rho_z/\rho_x$, and the limits of z are from 0 to t. We now define a variable substitution given by $z_{\mathrm{eff}} = z\sqrt{\xi}$ and substitute this into equation (2) to find

$$(\partial^2 V/\partial x^2) + \left(\partial^2 V \big/ \partial z_{\mathrm{eff}}^2\right) = 0. \tag{3}$$

Equation (3) is Laplace's equation for an isotropic material where the limits of z_{eff} are now from 0 to the effective thickness, $t_{\mathrm{eff}} = t\sqrt{\xi}$. A single variable t_{eff} is therefore used to account for both sample thickness and material anisotropy in the following analysis.

2.2. Interface resistance

Interface resistance (R_c), the resistance of the electrode–sample interface, is incorporated into the FE model through the boundary conditions (BCs) applied at the electrodes. All contacts are assumed to have the same R_c, which is independent of the applied potential. An interface resistance factor (α) is defined by $\alpha = R_c \big/ R_{ij}^{kl}$.

2.3. Electrode configuration

In 4-probe electrical transport measurements, the outer electrodes are typically connected to a current source and the inner electrodes to a high impedance voltmeter ($R_{14}^{23} = V_{23}/I_{14}$, see figure 1). The reciprocity principle states that for a network of linear resistors, an electromotive force (emf) in one branch of the network will produce the same current in the other branches as an equivalent circuit where the emf has been moved to another branch [18, 19]. Thus for a linear system (i.e. linear *I–V* dependence of the sample and interface), the electrode arrangement in figure 1 is equivalent to the reverse configuration $\left(R_{14}^{23} = R_{23}^{14}\right)$ where the inner electrodes are the current terminals and the outer electrodes measure the resulting potential drop. In this work only the electrode configuration shown in figure 1 is considered.

Table 1. Dimensionless variables used in all analyses.

The effective thickness ratio	$TR_{\text{eff}} = t\sqrt{\xi}/s$
The electrode ratio	$ER = \Delta/s$
Interface resistance factor	$\alpha = R_c/R_{ij}^{kl}$

Table 2. The boundary conditions implemented in the FE model for the source and sense electrodes.

No	Description	Source electrode		Sense electrode	
1	Moderate interface resistance	$\mathbf{n}\cdot\mathbf{J} = \frac{V_+ - V(x,t)}{R_c w \Delta}$	(4)	$\int_{\partial\Omega} \mathbf{n}\cdot\mathbf{J} = 0$, $\mathbf{n}\cdot\mathbf{J} = \frac{V(x,t)-V_s}{R_c w \Delta}$	(5) (6)
2	Perfect contact ($\alpha = 0$)	$V(x,t) = V_+$	(7)	$\int_{\partial\Omega} \mathbf{n}\cdot\mathbf{J} = 0$	(5)
3	Large interface resistance ($\alpha \gg 1$)	$\mathbf{n}\cdot\mathbf{J} = \frac{I_{ij}}{w\Delta}$	(8)	$\mathbf{n}\cdot\mathbf{J} = 0$	(9)

2.4. Definition of variables

For samples with finite-width electrodes, it is non-trivial to define an appropriate inter-electrode spacing that properly defines the distance of the measured potential drop. In this work the inter-electrode spacing (s) is defined as the distance between the inner edges of neighbouring electrodes, as shown in figure 1. The inter-electrode spacing is also used as the characteristic length scale with respect to which the remaining geometric variables are defined. All the dimensionless variables used in this work are listed in table 1.

2.5. The finite element model

The current density and potential distributions within the sample are symmetric about the centreline ($x = 0$, see figure 1), so only half of the specimen geometry needs to be modelled. The centreline is constrained to be an electrical ground. All the remaining boundaries, with the exception of the source (current) and sense (potential) electrodes, are modelled as electrically insulating ($\mathbf{n}\cdot\mathbf{J} = 0$, where $\mathbf{n}$ is the unit vector normal to the boundary).

All electrodes are assumed to have a conductivity that is much greater than the sample conductivity and are treated as equipotential. In this work, the electrodes and interfaces are not directly modelled. Their effect is included in the FE model via appropriate BCs. Six BCs, listed in table 2, are used to model the full range of possible interface resistances including the general case for moderate R_c as well as the limiting cases of perfect contact ($\alpha = 0$) and very large interface resistance ($\alpha \gg 1$).

In the general case for moderate values of interface resistance (table 2, case 1), a potential drop occurs when current passes though the sample–electrode interface. For the source electrode, this effect is modelled using equation (4) where V_+ is the potential applied to the source electrode (an input parameter) and $V(x, t)$ is the potential on the sample surface. Application of this nonlinear BC leads to a non-uniform distribution of current injected into the sample at the source electrode. At the sense electrode, a portion of the sample current passes through the equipotential electrode resulting in a potential drop across the interface. This effect is accounted for in the FE model by applying equations (5) and (6) simultaneously at the boundary, where V_s is the potential of the sense electrode (a variable in the FE model). The application of equation (5) to the boundary allows some current in the sample to be diverted locally through the less resistive electrodes, but ensures that the total current flowing across the boundary is 0.

In the limiting case where the sample and the electrodes are in perfect contact ($\alpha = 0$, table 2, case 2), the potential on the sample surface under the electrodes will be constant and equal to that of the electrode. In this regime the boundaries of the source and sense electrodes are modelled using the *uniform potential*, equation (7), and *floating potential* BCs, respectively. The floating potential BC sets the potential of the boundary equal to a constant that is determined by applying equation (5) at the boundary. The floating potential BC is a built-in boundary condition in Comsol Multiphysics 3.2.

At the opposite limit, where $\alpha \gg 1$ (table 2, case 3), the large interface resistance impedes current from flowing through the highly conductive electrodes, thus decoupling the electrodes from the current and potential distributions in the sample. In this case the electrodes are modelled using the uniform current distribution, equation (8), and the electrical insulation, equation (9), BCs for the source and sense electrodes, respectively. The potential of the sense electrode, V_s, is assumed to be equal to an average of the potential on the sample surface under the sense electrode [8, 9]. The potential measured by the ith electrode whose mean position is located at x_i is given by

$$(V_s)_i = \frac{1}{\Delta_i}\int_{x_i-\Delta_i/2}^{x_i+\Delta_i/2} V(\varsigma, t)\,\mathrm{d}\varsigma, \tag{10}$$

where Δ_i is the width of the ith electrode and ζ is the variable of integration. The integral is evaluated by the Comsol Multiphysics program using element-wise fourth-order numerical quadrature.

The mesh is generated by a built-in algorithm in Comsol Multiphysics and consists of 2D six node (quadratic) triangular elements. An anisotropic mesh is used with mesh elements concentrated along the upper surface ($z = t$) and along the line of symmetry ($x = 0$). Convergence of the FE solution is ensured by using optimized mesh parameters and verified for $\alpha \gg 1$ by comparing the values of the applied current (I_{ij}) with the total current (I) found by evaluating the following relationship $I = w\int_0^t (\mathbf{n}\cdot\mathbf{J})\,\mathrm{d}y$ along the line of symmetry. The optimized mesh parameters are established by running the model several times with increasing mesh refinement until the solution converges. The total number of elements is a function of the geometry of the sample with the average number of elements varying from 5000 to 80 000 with an increasing sample area. The mesh is regenerated for each sample geometry.

The Comsol Multiphysics FE program is implemented in MATLAB 7.0.3 (Mathworks, Inc) allowing the FE calculation to be quickly carried out for a variety of sample geometries. The sample's 4-probe resistance is computed using $R = 2V_s/I$. The measured resistivity is found using equation (1), and the correction factor is found by calculating the ratio of the in-plane resistivity used in the model ($\rho_x = \rho = 1$) and the measured resistivity.

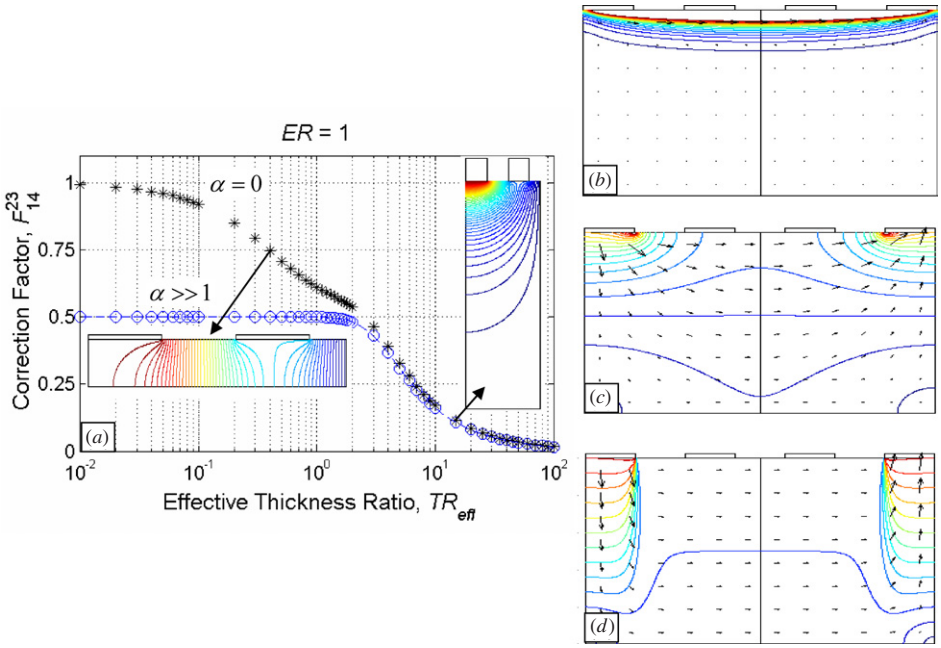

Figure 2. (*a*) Correction factor versus TR_{eff} for the limiting cases of perfect contact ($\alpha = 0$) and large interface resistance ($\alpha \gg 1$) for a sample with $ER = 1$. The dashed line is the analytical solution from equation (11). The contour plots are of the potential field distribution for $\alpha = 0$. The arrows pointing to the contour plots show the corresponding position on the F curve ($TR_{\text{eff}} = 0.4$ and 15). (*b*)–(*d*) Contour plots of the magnitude of the current density with an arrow plot superimposed showing the current flow for samples with $\alpha \gg 1$. The contour levels are identical for all plots, and the length of the arrows is proportional to the magnitude of the current density. Sample parameters are $ER = 1$ and $TR_{\text{eff}} = 50$ (*b*), 5 (*c*), 0.5 (*d*).

3. Simulation results and discussion

3.1. The effect of material thickness and anisotropy

As indicated above, the material anisotropy and the thickness of the sample are intimately linked. The contour plots in figure 2 illustrate the non-uniformity in the current density field that develops in a sample as its effective thickness increases. For large values of effective thickness ($TR_{\text{eff}} > 50$), the applied current is restricted to a thin layer near the sample surface (see figure 2(*b*)). The opposite is true for a sample with small effective thickness where the current now prefers to flow in the z-direction probing the entire depth of the sample (see figure 2(*d*)).

The non-uniformity of the current density field leads to a change of the correction factor. Figure 2(*a*) is a plot of F versus TR_{eff} for the limiting cases of perfect contact and large interface resistance. For samples with a large thickness compared to the inter-electrode spacing (i.e. $TR_{\text{eff}} > 2$ in figure 2(*a*)), F for both limiting cases steadily decreases with a slope of $1/TR_{\text{eff}}$ with increasing TR_{eff}. In this regime, the applied current only probes a portion of the sample volume near the surface (see figure 2(*b*)). For an infinitely thick sample, the depth reached by the applied current is dependent on the distance between the outer electrodes ($L = 3s + 4\Delta$). As TR_{eff} for a finite thickness sample increases beyond this depth ($t_{\text{eff}} > L$), the thickness of the probed volume remains constant (see the contour plot for $TR_{\text{eff}} = 15$ in figure 2(*a*)) causing a steady decrease in F.

An analytical solution for Laplace's equation with BCs that are identical to those used in the limiting case of $\alpha \gg 1$ (see table 2, case 3) has been derived elsewhere [8–10]. Using these results, an analytical expression for the correction factor is given by

$$F = \frac{1}{8\,(T\,R_{\text{eff}})}\,\frac{1}{\Lambda}\,, \tag{11}$$

where Λ is an infinite series having the following form:

$$\Lambda = \sum_{n=1,3,5,\ldots} (-1)^{n-1/2}\operatorname{sinc}\left(n\pi\,\frac{ER}{LR}\right)\operatorname{sinc}\left(n\pi\,\frac{ER}{2\,(LR)}\right) \times \frac{\sin\left[\frac{n\pi}{2(LR)}\,(ER+1)\right]}{n\pi}\coth\left(\frac{n\pi\,(T\,R_{\text{eff}})}{LR}\right)\,. \tag{12}$$

In equation (12), LR is the length ratio (L/s) for the specimen, which can be expressed in terms of ER by $LR = 3 + 4ER$. The dashed lines in figures 2(*a*) and 5 represent the analytical solution from equation (11). The FE and analytical results show excellent agreement in the limiting case of $\alpha \gg 1$ for all values of TR_{eff} and ER.

3.2. The effect of interface resistance

The effect of interface resistance on the potential field distribution in the specimen is shown in figure 3. When the electrode and sample are in perfect contact ($\alpha = 0$), the surface of the specimen is forced to be at the same potential as the electrode, perturbing the linear distribution of the potential field (see figure 3(*a*)). The gradient of the potential is increased near the edges of the electrodes due to current passing into or out of the highly conductive electrodes. In this regime, the current applied to the sample flows along the source electrode and is injected into the sample near the electrode edge. As the interface resistance increases, the effect

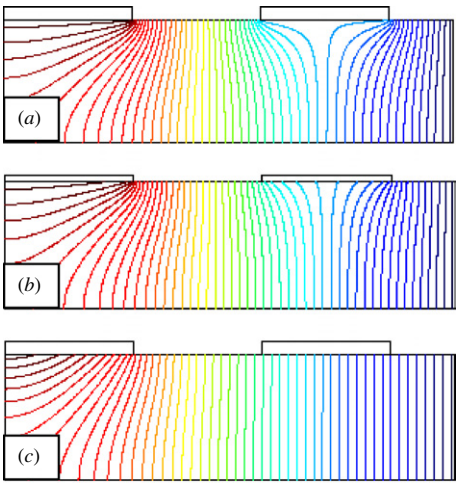

Figure 3. Potential contour plots for an isotropic material ($\xi = 1$) with $ER = 1$ and $TR_{\text{eff}} = 1$. The interface resistance increases from top to bottom: (*a*) $\alpha = 0$, (*b*) $\alpha = 0.1$ and (*c*) $\alpha \gg 1$.

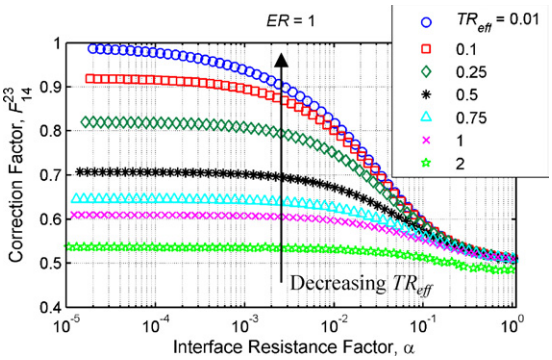

Figure 4. Correction factor versus interface resistance factor for several values of TR_{eff} and at $ER = 1$, showing the transfer of the correction factor between the limiting cases of perfect contact and large interface resistance.

of the perturbation of the equipotential electrodes on the potential field decreases (see figure 3(*b*)). In the limiting case, where $\alpha \gg 1$, the electrodes are fully decoupled from the sample, and the potential field has a linear distribution that is constant through the thickness for a large portion of the sample volume (see figure 3(*c*)) approximating the potential distribution assumed in equation (1).

A comparison of the contour plots in figure 3 shows that interface resistance has a significant impact on the potential field distribution in the specimen, which can be accounted for by F. Figure 2(*a*) is a plot of F versus TR_{eff} for both limiting cases of $\alpha \gg 1$ and $\alpha = 0$. For thin samples ($TR_{\text{eff}} < 2$, when $ER = 1$), the difference in the value of F for the limiting cases is due to a difference in the current flow in the sample; when $\alpha \gg 1$ (see figure 3(*c*)) all of the current remains in the sample, and when $\alpha = 0$ (see figure 3(*a*)) some current is diverted through the electrodes.

For moderate values of α, the correction factor transitions between the limiting cases (see figure 4). This transition occurs over five orders of magnitude with perfect contact being approximated by $\alpha < 10^{-5}$ and the large interface

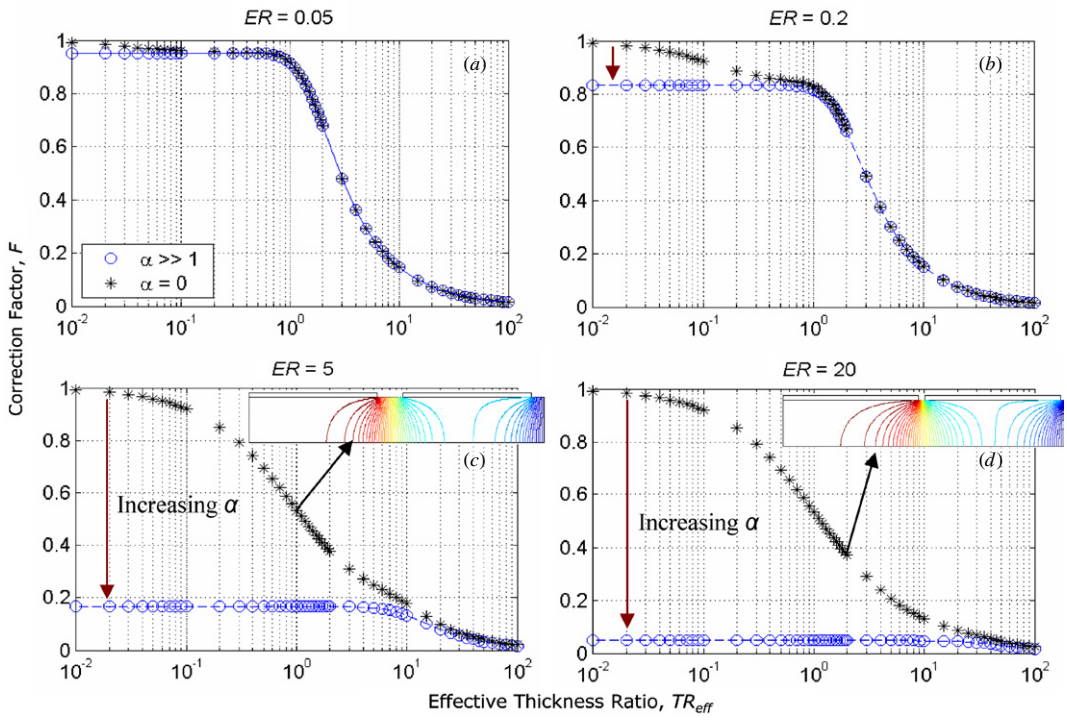

Figure 5. Correction factor versus TR_{eff} for the limiting cases of perfect contact and large interface resistance. ER of the samples is (*a*) 0.05, (*b*) 0.02, (*c*) 5 and (*d*) 20. The dashed line in each plot is the analytical solution from equation (11). The contour plots in (*c*) and (*d*) are of the potential field for a sample with $\alpha = 0$ and $TR_{\text{eff}} = 1$ and 5, respectively. The arrows pointing to each contour plot originate from the corresponding position on the F curve.

resistance limit occurring at $\alpha \approx 1$. With increasing TR_{eff}, the values of F for all values of α converge. This is caused by a decrease in the volume of the sample affected by the equipotential electrode with increasing TR_{eff}, which is evident by comparing the contour plots in figure 2(*a*).

3.3. The effect of the electrode size

The effect of the electrode size on F in the limiting cases of perfect contact and large interface resistance is shown in figure 5. For thin samples where $TR_{\text{eff}} < 0.1$, regardless of the size of the electrodes, F approaches a constant value for both limiting cases. The correction factor approaches a value of 1 in the limiting case of perfect contact. In this regime (i.e. $\alpha = 0$), the equipotential electrodes force the potential field in the sample under the electrode to be equipotential through the thickness (see the contour plot in figure 5(*c*)), effectively short circuiting the sample volume under the electrode [20]. The distance of the measured potential drop is therefore defined by the geometric inter-electrode spacing, s.

In the limit of large interface resistance, the potential of the sense electrode is assumed to be equal to an average of the potential on the sample surface under the electrode given by equation (10). In this regime the potential field at the sample surface varies linearly (see figure 3(*c*)), so the potential of the sense electrode can be approximated by the potential on the sample surface at the mid-point of the electrode [8]. Therefore the region of the measured potential drop for samples where $\alpha \gg 1$ is between the centres of the inner electrodes, and the appropriate inter-electrode spacing to use when computing the sample resistivity is $s_{\text{eff}} = s(ER + 1)$, where s_{eff} is the effective inter-electrode spacing. The dependence of the effective inter-electrode spacing on the electrode width in the limit of $\alpha \gg 1$ causes the magnitude of F for thin samples ($TR_{\text{eff}} < 1$) to be equal to $1/(ER + 1)$ (see figures 2(*a*) and 5). For moderate values of α, the effective inter-electrode spacing transitions from the inner edges to the midpoint of the inner electrodes with increasing α.

The range of TR_{eff} and F over which the limiting cases converge is also dependent on ER (see figures 2(*a*) and 5). When the sample and electrodes are in perfect contact ($\alpha = 0$), the volume of the sample that is affected by the equipotential electrodes increases with increasing ER. This is evident by comparing the contour plots in figures 5(*c*) and (*d*), which have a similar potential field distribution; however, ER and TR_{eff} differ by a factor of 4 and 5, respectively. When $\alpha \gg 1$, the dependence of the effective inter-electrode spacing, s_{eff}, on ER affects the depth with which the applied current probes the sample causing a shift in F along the TR_{eff} axis. The combination of these effects delays the convergence of the limiting cases to larger values of TR_{eff}. Thus, the importance of accounting for the effects of the interface resistance becomes ever greater as the width of the electrodes increases.

4. Conclusions

We have presented a self-consistent finite element (FE) approach that is used to determine correction factors that convert the resistivity obtained from a co-linear 4-probe electrical measurement of sample resistance and sample–electrodes geometry into the *true* material resistivity. A variety of effects were included in the FE model: material anisotropy, sample geometry and the sample–electrode interfaces. Interface resistance was included in the model through the use of appropriate boundary conditions for the source (current) and sense (potential) electrodes. In this work the FE approach is used to investigate the effects of anisotropic material properties, interface resistance and electrode size on the correction factor for small, highly resistive samples with large, closely spaced, highly conductive electrodes that extend across the sample width. The results of the FE analysis show the following.

(1) Anisotropic electrical properties lead to a change in the thickness of the sample that is probed by the applied current. A substitution of the variable is defined where $z_{\text{eff}} = z\sqrt{\xi}$, to account for anisotropic material properties in the FE model.
(2) Large and highly conductive electrodes perturb the potential and current density distributions in the sample. The effect of this perturbation on the correction factor is dependent on the size of the electrodes, the interface resistance and the thickness of the sample.
(3) Interface resistance can have a significant effect on 4-probe electrical transport measurements, particularly for samples whose thickness is less then $s + \Delta$.
(4) In the limiting cases of perfect contact and large interface resistance, the distance that defines the measured potential drop is between the inner edges (s) and centre ($s + \Delta$) of the inner electrodes, respectively. The distance for the measured potential drop transitions from the inner edge to the centre of the inner electrodes with increasing interface resistance relative to the sample resistance.
(5) The FE model showed excellent agreement with analytical results in the limit of large interface resistance. The expression for the correction factor given by equation (11) can be used with reasonable accuracy for samples where the interface resistance is of the same order as the sample resistance.

In future work our FE approach could be used to evaluate other effects on the correction factor including changes in the resistivity due to temperature variations, different physics that may occur at the interface between the electrode and sample, etc. The methods outlined in this paper can also be applied to 4-probe heat transport measurements. Our FE approach and the results of our analysis will help improve the accuracy of electrical transport measurements for many materials.

Acknowledgments

We are thankful to V Chandrasekhar (NU), J Ketterson (NU) and E Danielsson (Comsol, AB) for valuable discussions. We gratefully acknowledge the NASA University Research, Engineering and Technology Institute on Bio Inspired Materials (BIMat; No. NCC-1-02037) and the National Science Foundation (No. CMS-0304506).

References

[1] Schroder D K 1998 *Semiconductor Material and Device Characterization* 2nd edn (New York: Wiley)

[2] Valdes L B 1952 Effect of electrode spacing on the equivalent base resistance of point-contact transistors *Proc. IRE* **40** 1429–34
[3] Valdes L B 1954 Resistivity measurements on germanium for transistors *Proc. IRE* **42** 420–7
[4] Uhlir A 1955 The potentials of infinite systems of sources and numerical solutions of problems in semiconductor engineering *Bell Syst. Tech. J.* **34** 105–29
[5] Smits F M 1958 Measurement of sheet resistivities with the four-point probe *Bell Syst. Tech. J.* **37** 711–8
[6] Shi J S and Sun Y C 1997 New method of calculating the correction factors for the measurement of sheet resistivity of a square sample with a square four-point probe *Rev. Sci. Instrum.* **68** 1814–7
[7] Weller R A 2001 An algorithm for computing linear four-point probe thickness correction factors *Rev. Sci. Instrum.* **72** 3580–6
[8] Busch R, Ries G, Werthner H, Kreiselmeyer G and Saemannischenko G 1992 New aspects of the mixed state from 6-terminal measurements on $Bi_2Sr_2CaCu_2O_X$ single-crystals *Phys. Rev. Lett.* **69** 522–5
[9] Levin G A 1997 On the theory of measurement of anisotropic electrical resistivity by flux transformer method *J. Appl. Phys.* **81** 714–8
[10] Esposito M, Muzzi L, Sarti S, Fastampa R and Silva E 2000 Determination of the resistivity components rho[ab] and rho[c] from multiterminal measurements in $Bi_2Sr_2CaCu_2O_{8+x}$ crystals *J. Appl. Phys.* **88** 2724–9
[11] Pierson H O 1993 *Handbook of Carbon, Graphite, Diamond and Fullerenes: Properties, Processing, and Applications* (Park Ridge, NJ: Noyes)
[12] Yoffe A D 1973 Layer compounds *Ann. Rev. Mater. Sci.* **3** 147–70
[13] Jiang C N, Baldwin A R, Levin G A, Stein T, Almasan C C, Gajewski D A, Han S H and Maple M B 1997 Nonmonotonic evolution of out-of-plane resistivity with Pr doping in $Y_{1-x}Pr_xBa_2Cu_3O_{7-\delta}$ single crystals *Phys. Rev.* B **55** R3390–3
[14] Steendijk P, Mur G, Vandervelde E T and Baan J 1993 The 4-electrode resistivity technique in anisotropic media—theoretical-analysis and application on myocardial tissue in-vivo *IEEE Trans. Biomed. Eng.* **40** 1138–48
[15] Wang Y Q, Schimpf P H, Haynor D R and Kim Y 1998 Geometric effects on resistivity measurements with four-electrode probes in isotropic and anisotropic tissues *IEEE Trans. Biomed. Eng.* **45** 877–84
[16] Park J B, Okabe T and Takeda N 2003 New concept for modeling the electromechanical behavior of unidirectional carbon-fiber-reinforced plastic under tensile loading *Smart Mater. Struct.* **12** 105–14
[17] Stankovich S, Dikin D A, Dommett G H B, Kohlhaas K M, Zimney E J, Stach E A, Piner R D, Nguyen S T and Ruoff R S 2006 Graphene-based composite materials *Nature* **442** 282–6
[18] Bleaney B I B B 1965 *Electricity and Magnetism* 2nd edn (Oxford: Oxford University Press)
[19] Hyun S, Thorpe M F, Jaeger M D, Golding B and Day A R 1998 Resistivity determination from small crystallites *Phys. Rev.* B **57** 6697–705
[20] Mak L K, Rogers C M and Northrop D C 1989 Specific contact resistance measurements on semiconductors *J. Phys. E: Sci. Instrum.* **22** 317–21